DOI: https://doi.org/10.15625/0868-3166/21108

Design of high efficiency and wideband dual-functional metasurface for polarization conversion and asymmetric transmission

Dinh Dat Nguyen¹, Van Nhan Pham¹, Dinh Lam Vu², Thi Quynh Hoa Nguyen^{1,†}

E-mail: †ntqhoa@vinhuni.edu.vn

Received 9 July 2024 Accepted for publication 9 September 2024 Published 29 October 2024

Abstract. A wideband and high-efficiency bi-functional metasurface for polarization conversion and asymmetric transmission based on the gratings/polarization converter/gratings structure is proposed. The metasurface structure consists of a two double-split ring structure array sandwiched by two orthogonal metallic sub-wavelength gratings. Using two orthogonal metallic sub-wavelength gratings, the proposed metasurface reveals excellent asymmetric transmission effect and nearly perfect polarization conversion performance for linearly polarized waves. The proposed metasurface achieves a polarization conversion ratio of above 0.99 from 3.7 GHz to 20.2 GHz with a relative bandwidth of 138% and an asymmetric transmission parameter exceeding 0.9 from 5.8 GHz to 17 GHz with an relative bandwidth of 99.5%. Moreover, the proposed metamaterial maintains high polarization conversion ratio and asymmetric transmission performance for a wide range of incident angles. Due to its outstanding features, including wideband and high efficiency in both polarization conversion ratio and asymmetric transmission performance, this bifunctional metasurface holds promise for applications in polarization imaging, radar, radiometer, and transmission array antenna.

Keywords: polarization conversion; asymmetric transmission; metasurface.

Classification numbers: 81.05.Xj; 78.67.Pt.

©2024 Vietnam Academy of Science and Technology

¹School of Engingeering and Techonology, Vinh University, 182 Le Duan, Vinh, Vietnam

²Graduate University of Science and Technology, Vietnam Academy of Science and Technology, 18 Hoang Quoc Viet, Hanoi 10072, Vietnam

1. Introduction

Manipulating electromagnetic (EM) wave has great attention owing to their applications in optical and electric devices [1,2]. Traditional methods for manipulating EM wave polarization, such as the optical activity of crystals [3], the birefringence effect of anisotropic materials [4,5], and the Faraday effect [6], are limited to natural materials. However, these methods have several drawbacks, including large volume, low polarization conversion ratio (PCR), narrow relative bandwidth, and sensitivity to incidence angle, making them unsuitable for many real-world applications [2,7–9].

Metasurfaces are artificial two-dimensional materials with periodic or aperiodic subwavelength structures that offer unique advantages in controlling EM wave polarization due to their simple structure, lightweight, thin profile, and low loss [7]. Generally, metasurface-based polarization converters can be designed to operate in either transmission or reflection modes. However, transmissive polarization converter metasurfaces are still limited by narrow relative bandwidth and sensitivity to incident angles [7].

Recently, the asymmetric transmission (AT) effect, which is assisted by polarization conversion in a metasurface, has emerged as a significant topic for novel applications in non-reciprocal optical devices [2]. The asymmetric transmission (AT) effect, a Lorentz reciprocal phenomenon, acts similarly to a diode, making it suitable for using in direction-dependent polarization converters and polarization-controlled devices in polarization-sensitive sensing and imaging [10]. Therefore, some design approaches have been proposed such as using twisted pairs of polarization conversion resonators [2, 11–13] and gratings/polarization converter/gratings (GPG) structures [10, 14–19]. However, compared to GPG structures, current twisted-pair metasurface structures typically operate within a narrow frequency range. Therefore, many metasurface-based GPG structures have been developed to design the wideband AT effect. However, the wave function of a metasurface is inherently fixed and restricted to a narrow frequency range. Consequently, the development of wideband and multifunctional features for metasurfaces is still under exploration to surmount the obstacles impeding their practical applications in highly efficient polarization manipulating devices.

In this paper, we present a simple design for a high-efficiency, wideband bi-functional metasurface for asymmetric transmission and polarization conversion based on a gratings-polarization converter-gratings structure. Utilizing two orthogonal metallic sub-wavelength gratings, the proposed metasurface reveals excellent AT effect and nearly perfect polarization conversion performance for linearly polarized waves. Moreover, the high efficiency and wideband AT and PCR features of the proposed bi-functional metasurface are maintained over a wide incident angle, making it suitable for potential applications in polarization imaging, radar, radiometer, and transmission array antenna.

2. Structure design and method

Figure 1 shows the schematic diagram of the proposed bi-functional metasurface. The metasurface is based on the gratings-polarization converter-gratings structure, consisting of a metallic two double-split ring (DSR) structure sandwiched by two orthogonal metallic sub-wavelength gratings, as shown in Figs. 1(b)-(d). The Teflon (PTFE) substrates with a dielectric

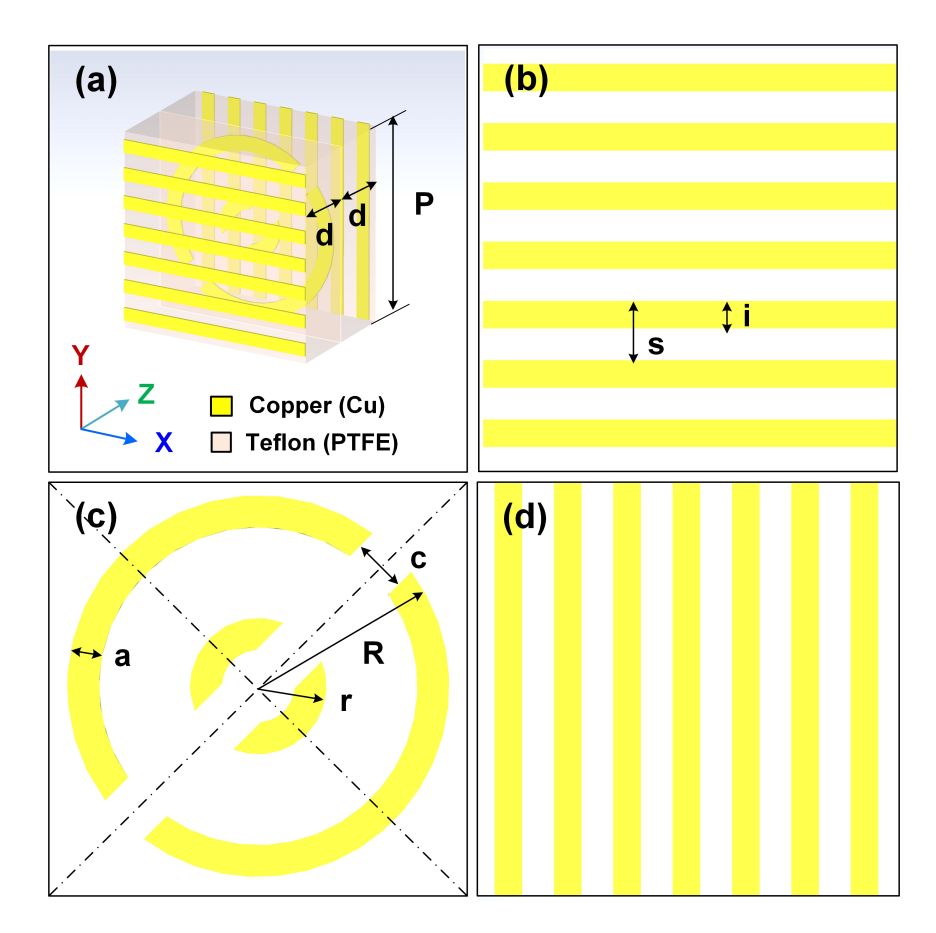


Fig. 1. The schematic view of the proposed bi-functional metasurface: (a) 3D-view unit cell, (b) top-view of a copper grating, (c) middle-view layer of two double-split rings metallic pattern, and (d) bottom-view layer of a copper grating.

constant of 2.1 and a loss tangent of 0.0002 are embedded between two layers. The metallic layers are made of copper with the conductivity $\sigma = 5.96 \times 10^7$ S/m and the thickness t = 0.035 mm.

In this work, the CST Microwave Studio software is used to optimize the design and evaluate the performance of the proposed bi-functional metasurface. In the simulation setup, unit cell boundary conditions are assigned for the x- and y-directions, while the open (add space) boundary condition is applied in the z-direction. The incident EM waves are linearly polarized for both forward y- and backward x-waves. Based on the simulation, the unit cell parameters of the bi-functional metasurface are optimized to achieve high efficiency and wideband characteristics. With the aid of simulation, the unit cell geometrical parameters of the proposed reconfigurable metasurface are optimized as follows: P = 9.1 mm, d = 3.0 mm, t = 0.035 mm, t = 0.035

It is important to note that the proposed bi-functional metasurface has overall unit cell dimensions of $9.1 \text{ mm} \times 9.1 \text{ mm} \times 6.105 \text{ mm}$, which can be manufactured using existing printed circuit board (PCB) processes. The top grating pattern is imprinted on the upper PTFE substrate,

while the DSR and bottom grating patterns are imprinted on the lower PTFE substrate, both having the same thickness of 3.0 mm. These two patterned PTFE substrates are then joined together to form the bi-functional metasurface structure, as shown in Fig. 1.

The relationship between the incident wave and transmitted wave can be expressed by the Jones matrix (T) given by [2, 11, 20]:

$$\begin{pmatrix} E_x^{tr} \\ E_y^{tr} \end{pmatrix} = \begin{bmatrix} t_{xx}^{f(b)} & t_{xy}^{f(b)} \\ t_{yx}^{f(b)} & t_{yy}^{f(b)} \end{bmatrix} \begin{pmatrix} E_x^{in} \\ E_y^{in} \end{pmatrix} = T_{lin}^{f(b)} \begin{pmatrix} E_x^{in} \\ E_y^{in} \end{pmatrix}, \tag{1}$$

where the superscripts f and b represent the propagation of the EM waves from forward (+z) and backward (-z), and the subscripts x and y denote the polarization direction of the EM waves, respectively.

To evaluate the linear polarization conversion (LPC) ability, a polarization conversion ratio (PCR) is calculated using the following formulas [2]:

$$PCR_{x} = \frac{|t_{yx}|^{2}}{|t_{yx}|^{2} + |t_{xx}|^{2}},$$
(2)

$$PCR_{y} = \frac{|t_{xy}|^{2}}{|t_{xy}|^{2} + |t_{yy}|^{2}},$$
(3)

$$T_{ij} = |t_{ij}|, (4)$$

where t_{ij} represents the transmission coefficient of the transmitted wave polarized in the *i* direction caused by the *j* polarized incident wave (i, j = x or y).

The asymmetric transmission (AT) parameter (Δ) of a linearly polarized wave is defined as the difference between the total transmission of forward propagation and that of backward propagation, which is used to measure the asymmetric transmission ability of the device and can be expressed as:

$$\Delta_{lin}^{x} = |t_{xx}^{f}|^{2} + |t_{yx}^{f}|^{2} - |t_{yx}^{b}|^{2} - |t_{xx}^{b}|^{2} = |t_{yx}^{f}|^{2} - |t_{xy}^{f}|^{2}, \tag{5}$$

$$\Delta_{lin}^{y} = -\Delta_{lin}^{x}. (6)$$

Furthermore, the PCR and AT performance are calculated through the relative bandwidth (RBW), which is calculated as Eq. (3) [21].

$$RBW = 2 \times \frac{f_H - f_L}{f_H + f_L},\tag{7}$$

where f_H and f_L are the highest and lowest frequency with PCR and AT efficiencies over 0.99 and 0.9, respectively.

3. Results and discussion

Figures 2(a) and (b) show the transmission coefficients for linearly polarized EM waves propagating along the forward (+z) and backward (-z) directions, respectively. The magnitudes of the cross-polarization transmission coefficients, t_{xy}^f and t_{yx}^b , exceed 0.9 from 5.6 to 17.4 GHz, with peak values above 0.995 at 6.26, 10.16, and 16.13 GHz. In contrast, the amplitudes of the co-polarization transmission coefficients, t_{xx}^f , t_{yy}^f , t_{xx}^b , and t_{yy}^b , are less than 0.02 within this frequency range. Additionally, the magnitudes of t_{yx}^f and t_{xy}^b are near zero across the entire frequency

range, indicating no polarization conversion for incident x-polarized (y-polarized) waves propagating along the -z (+z) direction. This suggests that the incident y-polarized (x-polarized) waves propagating along the +z (-z) direction are almost fully converted into transmitted x-polarized (y-polarized) waves within the wideband frequency range of 5.6 to 17.4 GHz. Conversely, there is no polarization conversion of incident x-polarized (y-polarized) waves along the +z (-z) direction throughout the entire frequency range.

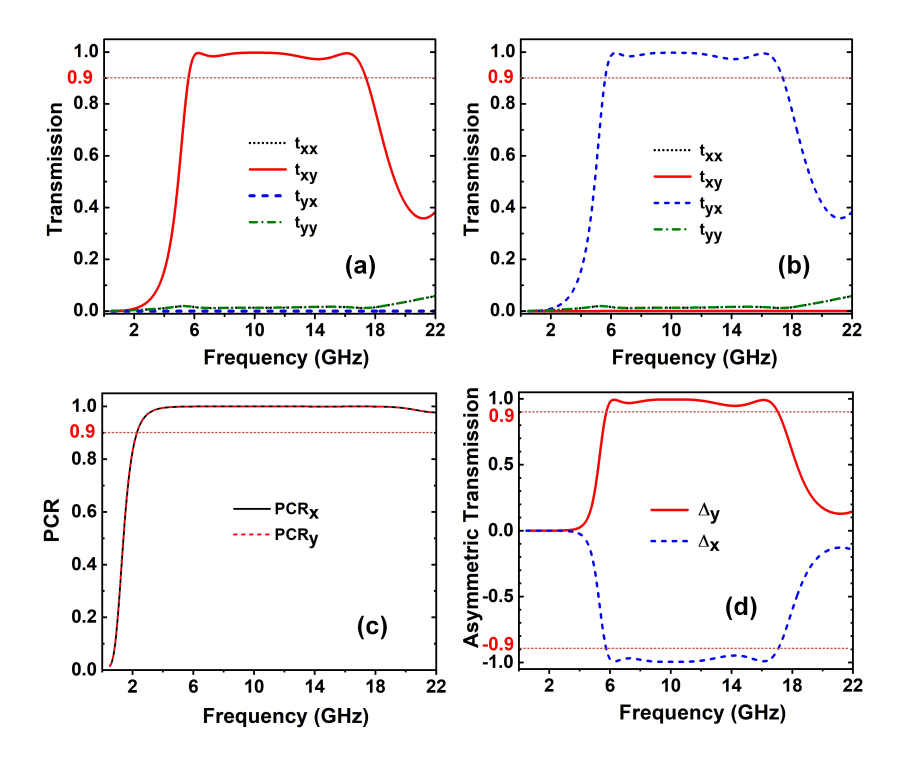


Fig. 2. Transmission coefficients under (a) forward and (b) backward incidence, (c) PCR for backward x-polarized wave (PCR $_x$) and forward y-polarized wave (PCR $_y$), and (d) AT parameter for forward y-polarized wave of the proposed bi-functional metasurface.

To evaluate the performance of the bi-functional metasurface, the PCR and AT spectra are simulated and presented in Figs. 2(c) and (d), respectively. The PCR depicts the conversion amount of one linearly polarized wave to another. Fig. 2(c) shows the PCR $_{x(y)}$ for the backward x-polarized wave and forward y-polarized wave. It can be seen that both PCR $_x$ and PCR $_y$ values exceed 99.9% across a wide bandwidth from 3.7 GHz to 20.2 GHz with an RBW of 138%. This indicates that the proposed metasurface achieves high efficiency and wideband polarization conversion, transforming linearly x-polarized (y-polarized) incident waves propagating along the -z (+z) direction into transmitted y-polarized (x-polarized) waves. As shown in Fig. 2(d), the AT characteristic is observed in the frequency range of 5.7–17 GHz with an AT value greater than 0.9 and an RBW of 98.2%. Thus, the proposed tri-layer metasurface structure reveals a giant AT effect for linearly polarized waves.

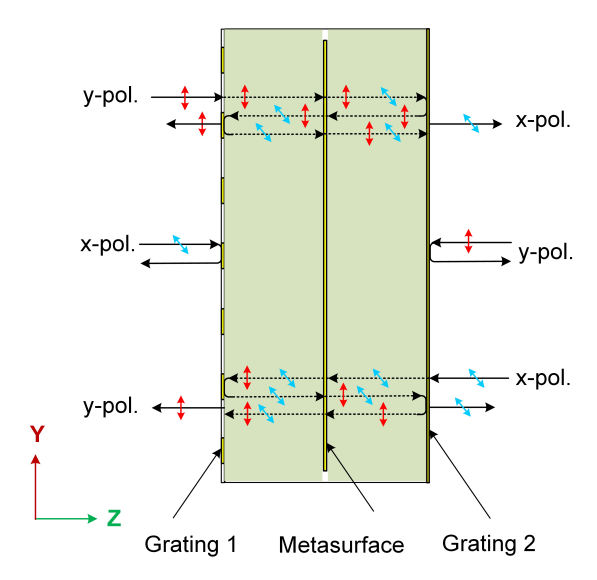


Fig. 3. The schematic of the grating-polarization converter-grating model.

To better understand the EM wave transmission in the tri-layer structure, a schematic of the Fabry-Perot-like resonance model is shown in Fig. 3. In this tri-layer system, the grating 1 and grating 2 layers can be regarded as *y*-polarization and *x*-polarization selectors, respectively, while the metasurface layer can play an important role in cross-polarization conversion (*y*-pol. to *x*-pol. and *x*-pol. to *y*-pol.) due to the diagonal symmetry of the designed metasurface structure [14]. Furthermore, diagonal symmetric metasurfaces have been reported to enable cross-polarization conversion in reflection mode [22, 23]. When an incident *y*-polarized EM wave impinges on the structure from the +*z* direction, it couples with grating 1 and then is converted into an *x*-polarized EM wave by the metasurface layer. This *x*-polarized EM wave then couples with the grating 2. Consequently, the incident *y*-polarized wave is nearly completely converted into an *x*-polarized wave when it passes through the tri-layer metasurface structure. It was reported that the performance of this structure, including its bandwidth and transmission efficiency, is directly impacted by the electrical properties of the metasurface layer and the dielectric losses caused by the dielectric spacer [24].

To elucidate the physical process of the polarization conversion, the electric field distributions in the cross-section of the metasurface at various resonant frequencies of 6.26 GHz, 10.16 GHz, and 16.13 GHz are simulated, as illustrated in Fig. 4. It can be observed that the y-polarized incident wave propagation along the forward (+z) direction converts into the x-polarized wave after passing through the tri-layer structure. Additionally, as shown in Figs. 4(a)-(c), the field patterns twisted inside the tri-layer metallic structure, which is due to the excitation of local resonant modes and inter-layer coupling among the tri-layer metallic structure at these resonant frequencies [2, 14, 15]. It has been reported that these phenomena arise from the anisotropic and chiral nature of the metasurface structure across various resonant frequencies [17]. Therefore, the presence of interlayer coupling and local resonant modes is the reason for the observation of the wideband cross-polarization conversion functionality in our proposed structure.

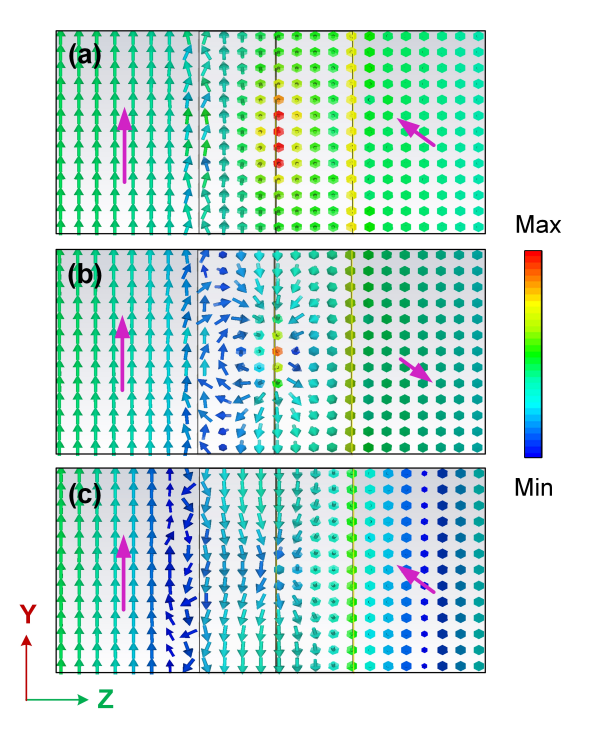


Fig. 4. Simulated electric field distribution in the cross-section of the proposed bifunctional metasurface for forward *y*-polarized wave at various frequencies of (a) 6.26 GHz, (b) 10.16 GHz and (c) 16.13 GHz. The arrows denote the electric field direction.

In practical applications, the incident wave is not always strictly perpendicular to the metasurface; therefore, the effect of incident angles on PCR and AT performance is investigated. As shown in Figs. 5(a) and (b), both PCR_x and PCR_y remain unchanged in the frequency range of 2-18.6 GHz with increasing the incident angle up to 60° . The wideband and high-efficiency PCR performance of the metasurface-based GPG structure can be sustained over a wide range of incident angles, which may be attributed to interlayer coupling. Meanwhile, the AT_y is almost unchanged expect a significantly reduce around 9.7 GHz, as depicted in Fig. 6. The appearance of this dip peak is due to a strong absorption. However, the proposed bi-functional metasurface maintains AT_y efficiency at 0.8 and 0.9 for incident angles up to 30° and 40°, respectively. These obtained results indicate that the proposed bi-functional metasurface has good PCR and AT performances across a wide range of incident angles.

Finally, to underscore the advanced nature of our work, we conducted a comparison of the functionalities, bandwidths, RBW, and efficiency of our proposed bi-functional metasurface structure with those of recently published studies, as summarized in Table 1. The data in Table 1 clearly demonstrate that our structure achieves the highest efficiencies and a moderate bandwidth for both dual LPC and AT functions. This suggests that our structure has significant potential for a wide range of microwave applications, including polarization imaging, radar, radiometer, and transmission array antenna.

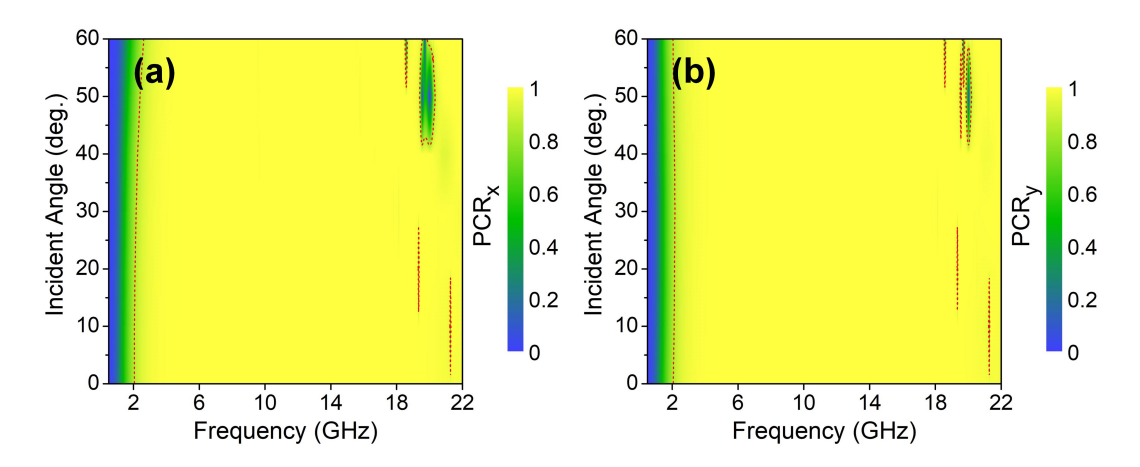


Fig. 5. (a) PCR efficiency as a function of incident angle for (a) forward y-polarized wave (PCR_y) and (b) backward x-polarized wave (PCR_x) of the proposed bi-functional metasurface. In figure plots the dash red contour curves indicated the 0.9 PCR efficiency.

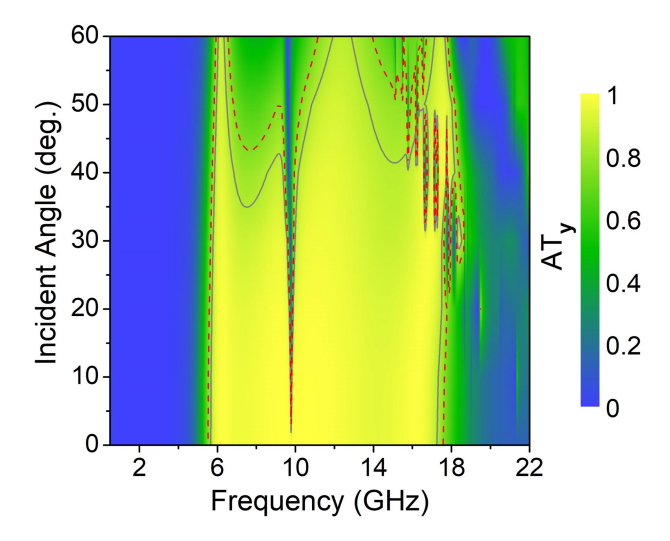


Fig. 6. AT efficiency as a function of incident angle for forward y-polarized wave (PCR_y) of the proposed bi-functional metasurface. In figure plots the black solid and dash red contour curves indicated the 0.9 and 0.8 AT efficiency, respectively.

4. Conclusions

A wideband and high-efficiency bi-functional metasurface for polarization conversion and asymmetric transmission based on the gratings-polarization converter-gratings structure was proposed, which is composed of a two-double-split ring structure array sandwiched by two orthogonal metallic sub-wavelength gratings. Using two orthogonal metallic sub-wavelength gratings, the proposed metasurface achieved excellent AT effect and nearly perfect polarization conversion

Reference	Function	Bandwidth (GHz)	RBW (%)	Efficiency
[17]	LPC	4.13–18	131.79	0.99
	AT	4.12-17.71	121.5	0.5
[25]	LPC	4.6–14.0	101.07	0.9
	AT	4.6-14.0	101.07	0.7
[15]	LPC	4.36-14.91	104.49	0.9
	AT	4.36-14.91	104.49	0.8
This work	LPC	3.7-20.2	138	0.99
	AT	5.8–17	91.5	0.9

Table 1. Performance comparison of the proposed bi-functional metasurface with existing works.

performance for linearly polarized waves. The proposed metasurface reveals the PCR of above 0.99 from 3.7 GHz to 20.2 GHz with an RBW of 138% and the AT parameter of over 0.9 from 5.8 GHz to 17 GHz with an RBW of 99.5%. Importantly, the high efficiency and wideband PCR and AT performances of the proposed bi-functional metasurface can be maintained for a wide range of incident angles. Therefore, this design can be applied for potential applications such as polarization imaging, radar, radiometer, and transmission array antenna.

Acknowledgements

This research is funded by Vietnam National Foundation for Science and Technology Development (NAFOSTED) under grant number 103.02-2021.44.

Authors contributions

T.Q.H.N. proposed the idea and prepared the manuscript. All authors contributed to the design and theoretical calculation and reviewed the manuscript.

Conflict of interest

The authors declare that they have no competing financial interests.

References

- [1] A. Arbabi, Y. Horie, M. Bagheri and A. Faraon, *Dielectric metasurfaces for complete control of phase and polarization with subwavelength spatial resolution and high transmission*, Nature Nanotechnology **10** (2015) 937.
- [2] Z. Wei, Y. Zhao, Y. Zhang, W. Cai, Y. Fan, Z. Wang et al., High-efficiency modulation of broadband polarization conversion with a reconfigurable chiral metasurface, Nanoscale Adv. 4 (2022) 4344.
- [3] C.-F. Hsieh, Y.-C. Lai, R.-P. Pan and C.-L. Pan, *Polarizing terahertz waves with nematic liquid crystals*, Opt. Lett. **33** (2008) 1174.
- [4] C.-Y. Chen, T.-R. Tsai, C.-L. Pan and R.-P. Pan, Room temperature terahertz phase shifter based on magnetically controlled birefringence in liquid crystals, Appl. Phys. Lett. 83 (2003) 4497.
- [5] K. Wiesauer and C. Jördens, *Recent advances in birefringence studies at thz frequencies*, Journal of Infrared, Millimeter, and Terahertz Waves **34** (2013) 663.
- [6] S. Ali, J. R. Davies and J. T. Mendonca, Inverse faraday effect with linearly polarized laser pulses, Phys. Rev. Lett. 105 (2010) 035001.

- [7] C. Fu, S. Dong, L. Liu, L. Zhang, W. Yu, X. Wang et al., Dual-broadband high-efficiency polarization conversion metasurface based on asymmetric transmission, Opt. Commun. 546 (2023) 129733.
- [8] Y. Qi, B. Zhang, C. Liu and X. Deng, *Ultra-broadband polarization conversion meta-surface and its application in polarization converter and rcs reduction*, IEEE Access 8 (2020) 116675.
- [9] M. Mutlu and E. Ozbay, A transparent 90° polarization rotator by combining chirality and electromagnetic wave tunneling, Appl. Phys. Lett. **100** (2012) 051909.
- [10] J.-S. Li and F.-Q. Bai, Dual-band terahertz polarization converter with high-efficiency asymmetric transmission, Opt. Mater. Express 10 (2020) 1853.
- [11] Y. Zhao, R. Yang, Y. Wang, W. Zhang and J. Tian, Vo₂-assisted multifunctional metamaterial for polarization conversion and asymmetric transmission, Opt. Express 30 (2022) 27407.
- [12] Y. Fu, H. Cheng, J. Wu, Y. Li, Y. Dai, D. Wen et al., A multifunctional metasurface with asymmetric transmission and high-efficiency cross-polarization converter, J. Appl. Phys. 132 (2022) 223106.
- [13] Y. Wang, M. Wang, B. Wu, H. Liu and X. Wu, Strong chirality and asymmetric transmission effect in twisted bilayer α-MoO₃ in Terahertz band, Opt. Laser Technol. 174 (2024) 110581.
- [14] Y. Cheng, R. Gong and L. Wu, *Ultra-broadband linear polarization conversion via diode-like asymmetric trans*mission with composite metamaterial for terahertz waves, Plasmonics 12 (2016) 1113–.
- [15] Y. Cheng, J.-C. Zhao, X. Mao and R. Gong, Ultrabroadband diode-like asymmetric transmission and highefficiency cross-polarization conversion based on composite chiral metamaterial, Prog. Electromagn. Res. 160 (2017) 89.
- [16] W. Pan, Q. Chen, Y. Ma, X. Wang and X. Ren, *Design and analysis of a broadband terahertz polarization converter with significant asymmetric transmission enhancement*, Opt. Commun. **459** (2020) 124901.
- [17] J. Zhao, N. Li and Y. Cheng, Ultrabroadband chiral metasurface for linear polarization conversion and asymmetric transmission based on enhanced interference theory, Chin. Opt. Lett. 21 (2023) 113602.
- [18] N. Li, J. Zhao, P. Tang and Y. Cheng, Triple-broadband asymmetric transmission via cross-polarization conversion based on composite chiral metasurface structure, Opt. Commun. 560 (2024) 130445.
- [19] A. Ahmed, Q. Cao, M. I. Khan, G. Shah, F. Ahmed, M. I. Khan et al., An angular stable ultra-broadband asymmetric transmission chiral metasurface with efficient linear-polarization conversion, Phys. Scr. 99 (2024) 035519.
- [20] C. Menzel, C. Rockstuhl and F. Lederer, Advanced jones calculus for the classification of periodic metamaterials, Phys. Rev. A 82 (2010) 053811.
- [21] T. Q. M. Nguyen, T. K. T. Nguyen, D. T. Le, C. L. Truong, D. L. Vu and T. Q. H. Nguyen, Numerical study of an ultra-broadband and wide-angle insensitive perfect metamaterial absorber in the uv-nir region, Plasmonics 16 (2021) 1583.
- [22] J. Xu, R. Li, S. Wang and T. Han, *Ultra-broadband linear polarization converter based on anisotropic metasur-face*, Opt. Express **26** (2018) 26235.
- [23] H. L. Phan, T. Q. H. Nguyen and J.-M. Kim, Multi-functional wideband metasurface: Perfect absorber and linear to linear and linear to circular polarization converter, IEEE Access 12 (2024) 11664.
- [24] X. Gao, L. Singh, W. Yang, J. Zheng, H. Li and W. Zhang, Bandwidth broadening of a linear polarization converter by near-field metasurface coupling, Sci. Rep. 7 (2017).
- [25] X. Huang, X. Ma, H. Gao, L. Guo and X. Li, *Ultra-wideband linear-polarization conversion metasurface with high-efficient asymmetric transmission*, Appl. Phys. A **129** (2023) 278.